



This is a repository copy of *Measurements and modelling of the response of an ultrasonic pulse to a lithium-ion battery as a precursor for state of charge estimation*.

White Rose Research Online URL for this paper:
<https://eprints.whiterose.ac.uk/171997/>

Version: Accepted Version

Article:

Copley, R.J., Cumming, D., Wu, Y. et al. (1 more author) (2021) Measurements and modelling of the response of an ultrasonic pulse to a lithium-ion battery as a precursor for state of charge estimation. *Journal of Energy Storage*, 36. 102406.

<https://doi.org/10.1016/j.est.2021.102406>

Crown Copyright © 2021 Published by Elsevier Ltd. This is an author produced version of a paper subsequently published in *Journal of Energy Storage*. Uploaded in accordance with the publisher's self-archiving policy. Article available under the terms of the CC-BY-NC-ND licence (<https://creativecommons.org/licenses/by-nc-nd/4.0/>).

Reuse

This article is distributed under the terms of the Creative Commons Attribution-NonCommercial-NoDerivs (CC BY-NC-ND) licence. This licence only allows you to download this work and share it with others as long as you credit the authors, but you can't change the article in any way or use it commercially. More information and the full terms of the licence here: <https://creativecommons.org/licenses/>

Takedown

If you consider content in White Rose Research Online to be in breach of UK law, please notify us by emailing eprints@whiterose.ac.uk including the URL of the record and the reason for the withdrawal request.



eprints@whiterose.ac.uk
<https://eprints.whiterose.ac.uk/>

Title

Measurements and modelling of the response of an ultrasonic pulse to a lithium-ion battery as a precursor for state of charge estimation

Authors

R. Copley^a, D. Cumming^b, Y. Wu^b and R.S. Dwyer-Joyce^a.

^a *Leonardo Centre for Tribology, Department of Mechanical Engineering, University of Sheffield, Sheffield, UK;*

^b *University of Sheffield, Department of Chemical and Biological Engineering, Sheffield, UK.*

Abstract

Lithium-ion batteries change their internal state during cycles of charge and discharge. The state of charge of a lithium-ion battery varies during the charging cycle and depends on the internal structure of the components which may degrade with use. Estimation of the state of charge is commonly performed by battery management systems that rely on charge counting and cell voltage measurement. Determining the physical state of the battery components is challenging. Recently, the response of an ultrasonic pulse to a battery has been successfully correlated with both change in state of charge and state of health, the quality of the approach is now well established. This study assesses the qualities contained within an ultrasound signal response by investigating the behaviour of ultrasonic waves as they pass through the components in a layered battery structure, as those components change with battery charge. A model has been developed to understand the nature of the ultrasound response and the features that provide a particular characteristic. This is useful as two apparently identical batteries can produce very different ultrasonic responses. Detailed data analysis has been performed to find which combination of data comparisons provides the strongest correlation with state of charge and guides decisions about future use of battery monitoring using ultrasound. Finally, a smart peak selection method has been developed to ensure that regardless of the nature of the ultrasound response, state of charge measurements are optimised by ensuring the regions of signal with best battery charge correlation are identified. This can greatly help with the automation of the process in a sensor-based battery management system.

Keywords

Lithium-ion battery, ultrasonic sensing, state of charge

1. Introduction

Since their introduction in the 1990's, lithium-ion batteries have become increasingly popular in mobile power applications, from hand-held devices such as smart phones and tablets to electric vehicles. The success of the lithium-ion battery is due to its high energy density and operating voltage, the best energy-to-weight ratio, no memory effect and undergo only small amounts of discharge when not in use when compared to alternative battery technologies [1]-[3]. There are limitations with this technology; stress induced material damage, capacity fade and the potential for thermal runaway. With optimal usage a battery can support only a finite

number of charge/discharge cycles, improper use can lead to deterioration in battery performance and a shortening of lifespan ^[4].

To assist in the care of battery usage, battery management systems (BMS) have been developed to monitor battery status. Estimating the available capacity of a battery, referred to as state of charge (SoC), is an important feature of a BMS. There are various methods of estimating SoC, from measured values such as ampere hour counting and open circuit voltage to modelling approaches such as machine learning algorithms and electrochemical models. Each method has benefits and disadvantages, the measured values are simple to obtain for example, but contain greater estimation errors than modelling methods which contain lower estimation errors but are complex, requiring processing time/power ^[5]. This work focuses on the use of ultrasound (US) to provide some understanding into the complex nature of reflected waves that contain real-time state of charge information from the battery cell to estimate battery state of charge.

Ultrasonic battery monitoring is a well-established method of obtaining feature rich data from a battery. Each battery, regardless of chemistry or design, undergoes redistribution of density as a function of charge along with bulk moduli changes in anode and cathode layers ^{[6], [7]}. Many studies now exist that use ultrasound to exploit this, as well as the monitoring of battery ageing ^[8], gassing ^[9] and swelling ^[10]. A further advantage of this method is the simple application of a sensor at a low cost making it suitable for implementation into a BMS ^{[7], [11]}.

Ultrasound defines sound waves that are above the normal range of human hearing, generally referred to as frequencies greater than 20kHz ^[12]. Ultrasound waves are non-invasive and there is no requirement to introduce instrumentation into any body under exploration and importantly, ultrasound is non-destructive, so that the propagating sound waves creating only minor and non-permanent changes to the body at particle level. Typically, waves are pulsed using either/or a combination of, longitudinal waves (where the material vibration occurs parallel to the direction of travel) and shear waves (where the vibration occurs perpendicular to the direction of wave travel) ^[13].

Reflections occur when a wave encounters a material interface (Figure 1). The difference in material properties can be due to material density and elasticity which will affect the sound speed for these materials. Where there is a difference, the wave can partially or completely reflect, it is these reflections that provide insights into an otherwise inaccessible body. For this study longitudinal waves are used as they provide the strongest reflection response from liquid and solid material interfaces.

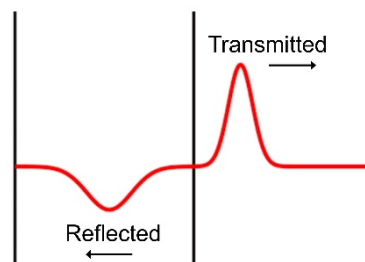


Figure 1: Example of a two layered body, when a wave encounters an interface (a change in material property) some part of the wave is transmitted and some is reflected.

Much of current ultrasound/battery studies have focused on improving accuracy by using pulse techniques and instrumentation experiments [7], [11], [14], [15]. Other studies have used ultrasound data combined with traditional SoC and state of health (SoH) estimation methods to reduce errors, as well as implementation in predictive models and machine learning algorithms [8], [14].

A common approach in most studies is the selection of a single peak in the time domain waveform, be that of an individual wave [8], [11], [16], [17] or from a signal envelope [14], [15]. From the time of flight (ToF) and signal amplitude, measurements are recorded and compared with battery information such as SoC and SoH. In previous work there is little discussion of the characteristics of the wave response and what causes it to return to the capturing sensor in the manner it does.

To this end, this paper focuses not on the accuracy of the method, but on the accuracy of the features within the ultrasound/SoC method. Potential challenges that are overcome with findings in this study include; combating the diverse nature of battery cell geometries which each may produce a different waveform response, assessing the effects of temperature changes from both external sources (ambient temperature) and internal (charge cycling temperature fluctuations) and the variance in quality of signal that could arise from instrumentation inconsistencies.

This paper will focus on two concepts; the various effects battery and pulsing parameters have and how these alter the nature of a wave response; and strategies to combat the diverse nature of battery cell geometries. The purpose of this study is to identify the most accurate and reliable waveform changes to correctly track battery changes with respect to state of charge.

2. Multilayered body model

2.1. Model background

A model was created to predict the transmission and reflection of a sound wave through a pouch cell represented as a 1D layered body. The passage of a 1D wave through a body is governed by the partial differential equation (PDE) wave equation

$$u_{tt} = c^2 u_{xx} \quad (1)$$

Where u is the wave position at point x and at time t , c is the wave speed through the material at position x . Differences in the wave speed c array will result in the transmission/reflection effect shown in Figure 1. The reflection coefficient is the proportion of a wave amplitude reflected at a boundary and is given by:

$$R = \frac{Z_2 - Z_1}{Z_2 + Z_1} \quad (2)$$

Where Z_n is the acoustic impedance of the material $Z_n = (\rho_n c_n)$, ρ being the material density and c being the sound velocity for the material. The reflection coefficient R varies between 0 and 1 and the transmission coefficient is $R-1$.

The boundaries are fixed and rather than c being a single constant wave speed value, it is built as an array with variable values to simulate differences in wave speed across the length of the body, modelling the properties of various material layers. As the wave encounters a different c value, some energy from the passing wave is transmitted and the rest is reflected, like that of the reflection coefficient R . The wave speed c is obtained using:

$$c = \sqrt{\frac{E}{\rho}} \quad (3)$$

Where E is the elastic modulus. A summary of the finite difference scheme is shown in Figure 2. By recording values adjacent to the model boundaries, simulated waveforms, such as those gained using contact transducers, are captured. The side with the initial pulse being a pulse/echo simulation and the opposing side simulating a pitch/catch through pulse.

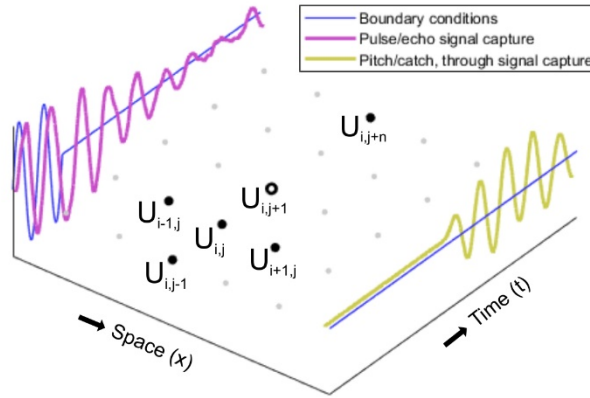


Figure 2: Finite difference scheme showing points in time/space used to calculate point $u_{i,j+1}$. Boundary conditions of left side include the initial pulse (blue). Position used to capture pulse/echo signal shown in magenta, pitch/catch through wave shown in yellow.

2.2. Model implementation

To model the ultrasonic wave passing through a simulated battery a matrix was created to represent the cell body in time and space. The length of time was specified (typically $20\mu\text{s}$ in steps of $dt = 2.7\text{ns}$ giving 7500 data points) and the cell body width (typically 5mm in steps of $dx = 20\mu\text{m}$ giving 250 data points). A base wave speed was set at $v=3000\text{m/s}$ to ensure the Courant–Friedrichs–Lewy (CFL) condition is met for model stability, where $CFL \leq 0.5$ from equation:

$$CFL = v \frac{dt}{dx} \quad (4)$$

The initial pulse was initialised in the time domain starting at $t=0$, being n number of consecutive sine waves (typically $n=3$). The wavelength was determined by setting a single sine wave to $1\mu\text{s}$ representing 1MHz , stacking and scaling these according to the user

requested cycle numbers and pulse frequency. The finite difference model calculated the wave position at each point across the cell body after which the time step was increased and the next iteration of the wave was calculated. The c array represents the wave speed across the battery, this varies simulating the various material properties of layers within the cell. Each block of identical wave speeds across the array represent the dimensions of each layer. As the wave encounters these changes in c the wave equation underpinning the model transmits and reflects proportions of the passing wave according the nature of the change in wave speed.

The wave speeds for the various components were generally taken from the density and elasticity values provided by Hsieh et al [6], calculated using equation (3) the layer dimensions were based on those provided by Ladpli et al [14]. Two separate matrices were generated where certain layers in the body alter in the time domain T to represent either stepped/partial or complete charge and discharge of the battery. This charge simulation used the range of density values for LiCoO₂ (cathode) and graphite (anode) and alters them linearly in multiple steps or a single step. The anode layer(s) decrease wave speed during charge whilst the cathode layer(s) increase wave speed. These localised layer density changes alter the nature of the wave reflections and provide differing wave responses, a simulated signal response, known as an A-scan, and Fourier transform are shown in Figure 3. Model animations are included in the supplementary material showing the propagation of the incident waves through the multiple layers of the cell generating A-scans (pulse/echo and pitch/catch) that result from the wave travelling through the specific material properties.

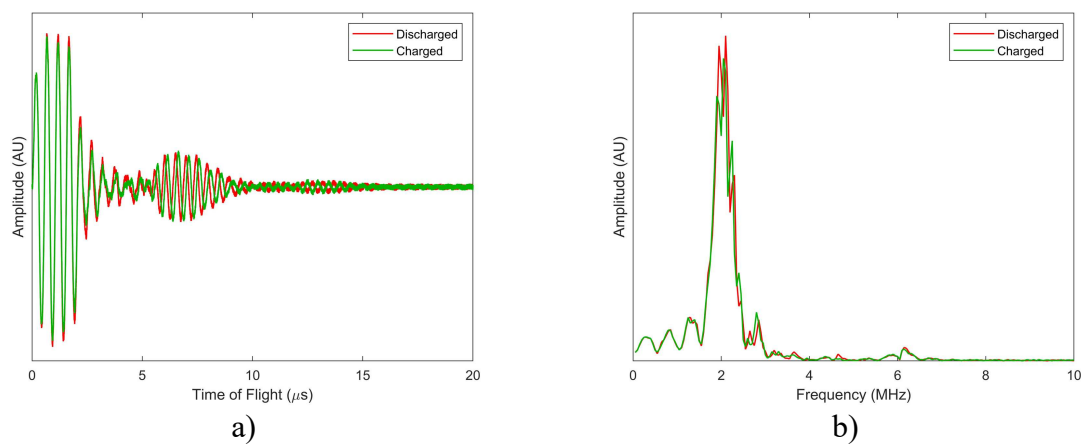


Figure 3: a) A-scan waveform generated by pulsing through the layers a simulated battery cell (red wave is discharged, green is charged state). b) Fourier transform for the simulation showing the main wave activity focused around the 2MHz region.

The speed of sound is temperature dependent. In the model, temperature effects are simulated by altering the wave speeds at a global rather than local level. The whole wave speed array c is raised and lowered uniformly according to a specified temperature profile, based on the assumption that temperature change would affect the cell body as a whole and uniformly. This provides an opportunity to observe change in ultrasound responses combining cell level changes (temperature) with localised battery layer changes (elasticity/density).

2.3. Illustration of model function

Figure 4 shows some sample output from the model at four time steps. The top half of each plot shows a different density distribution to the bottom half (although the overall density value remains unaltered) which can be thought of as charged/discharged states of a battery.

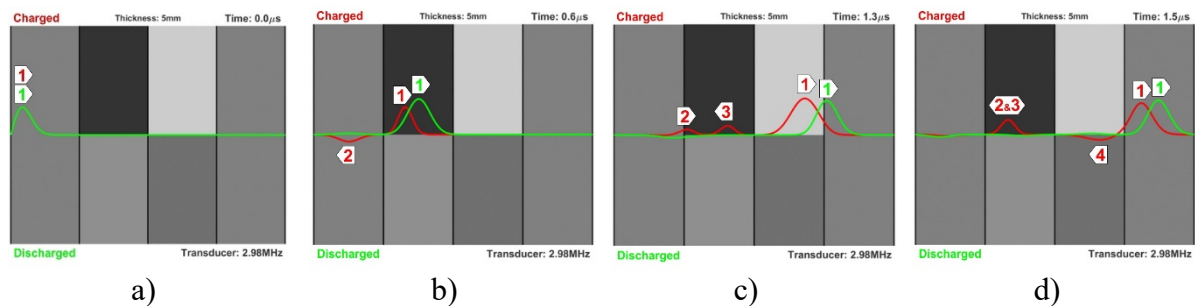


Figure 4: Simple four layered body wave model with differing density distribution. Notice due to the relatively even distribution of the theoretically discharged (bottom) half of the model, where the wave passes through layers with almost all the wave transmitted and very little reflection. These reflection/transmission events occur as every wave (including new waves) reaches each interface, in either direction. This causes the signal to quickly develop in complexity meaning direct measurements are difficult to take or unreliable.

For illustrative purposes, this simple case simulates four layers in a 5mm body thickness with an ultrasound sensor pulsing a single wave at a frequency of 3MHz. The timing of each capture is shown in the top right corner

- a) The model starts at $0.0\mu\text{s}$ and the two waves are overlaid with only the green, discharged state, wave visible.
- b) By $0.6\mu\text{s}$, the red wave (charged state) is only partially transmitted and some part of the wave is reflected back towards the source, in addition the red wave slows down somewhat and lags behind the green wave. This occurs as the red wave encounters a significant change in material property as this transmission/reflection effect occurs in such instances.
- c) By $1.3\mu\text{s}$ the red wave has passed through a second material property change and produced a third wave of note, reflected back towards the source, the second wave has reflected from the boundary and is now following behind the initial pulse.
- d) At $1.5\mu\text{s}$ both waves marked 2&3 pass through each other and form a constructed wave larger than each of the individual waves travelling through the body as they are of the same phase, by this time the incident wave has passed through a third layer interface and a new wave, wave 4 is reflected back towards the source. Notice the initial phase of waves 2 and 4 contrasted with wave 3, this is a result of change of material property values, 2 and 4 moved to a higher density material whilst wave 3 created as reflection traveling into a lower density material.

2.4. Ultrasound response to a typical battery structure

A typical pouch cell geometry configuration based on values in Table 1, with density and therefore wave speed values changing according to a battery charging profile, produces a series of simulated ultrasound wave responses that can be stacked to form the amplitude intensity plot shown in Figure 5a.

Component	Charge %	Elastic Modulus (GPa)	Density (kg/m ³)	Wave Speed (m/s)	Thickness (μm)	Citation
Anode (Graphite)	0	30	2078	3800	96	[6], [14]
	20		2213	3700		
	40	30	2348	3600	96	
	60		2484	3500		
	80		2619	3400		
Anode	100	30	2754	3300	96	[6], [14]
Separator		0.7	550	1128	25	[14]
Cathode (LiCoO ₂)	0	184	5663	5700	60	[6], [14]
	20		5488	5800		
	40	184	5312	5900	60	
	60		5137	6000		
	80		4961	6100		
Cathode	100	184	4786	6200	60	[6], [14]

Table 1: Elastic modulus and density values of electrodes and separator for ultrasonic wave response simulation.

Electrode material wave speeds increase/decrease as a function of the battery charging as lithium passes back and forth between anode and cathode during cycling. For the model, a constant current charge/discharge is considered, as such the density values move to their end values in a linear, incremental fashion. For more accurate modelling, changes in the elastic modulus should be included in calculations, however as with the model utilised by Hsieh et al. [6], the modulus is held constant and is considered sufficient for these estimation purposes.

The changes in density distribution cause ultrasonic wave response changes, stacking A-scans to form a signal intensity surface plot and synchronising with battery shows a clear relationship between charge and ultrasonic response.

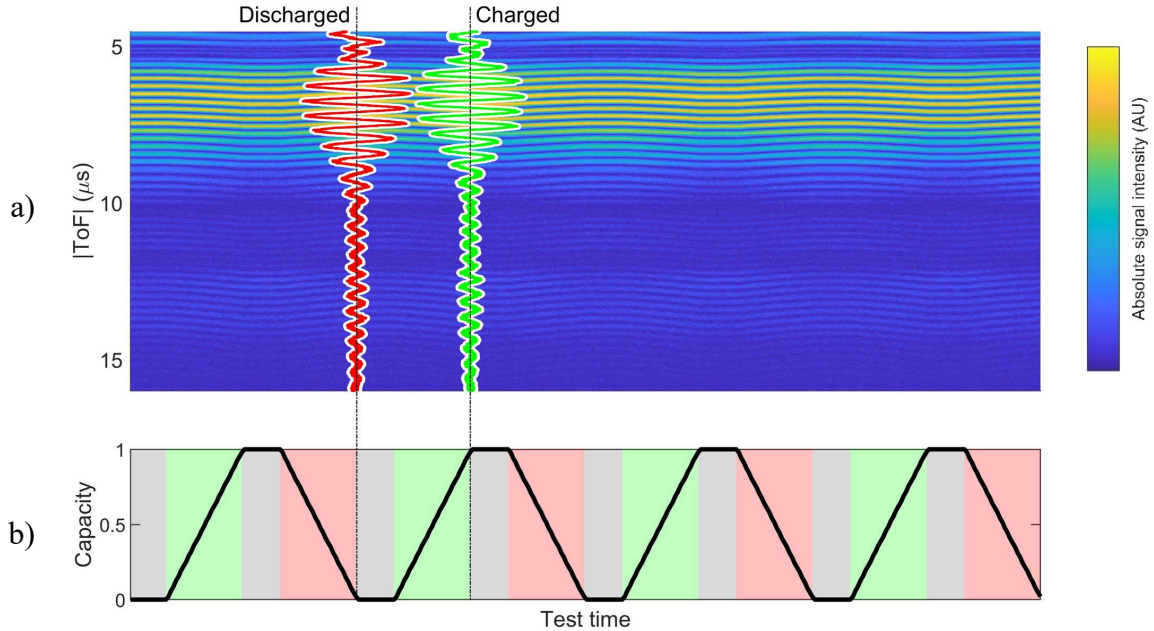


Figure 5: Predicted ultrasonic amplitude intensity map as a battery is charged and discharged. Each waveform (A-scan) is stacked (two sample signals shown, discharged state in red and charged state in green) to form a surface plot, where the high (yellow) intensity regions represent the larger amplitude signal peaks. The absolute values are shown in this plot for clearer viewing. In b) The battery capacity is plotted over a colour coded background to identify the part of the charge cycle (green = charge, red = discharge, grey = rest). The black dashed vertical lines show the position of the two sample waveforms.

2.5. Comparing battery geometries

The model is customisable, where the layout/stacking of active layers [cathode-separator-anode-separator] can be specified. The thicknesses of all layers and number of active layers can also be specified and the frequency and number of the initial pulses (2MHz and 2 cycles in this example).

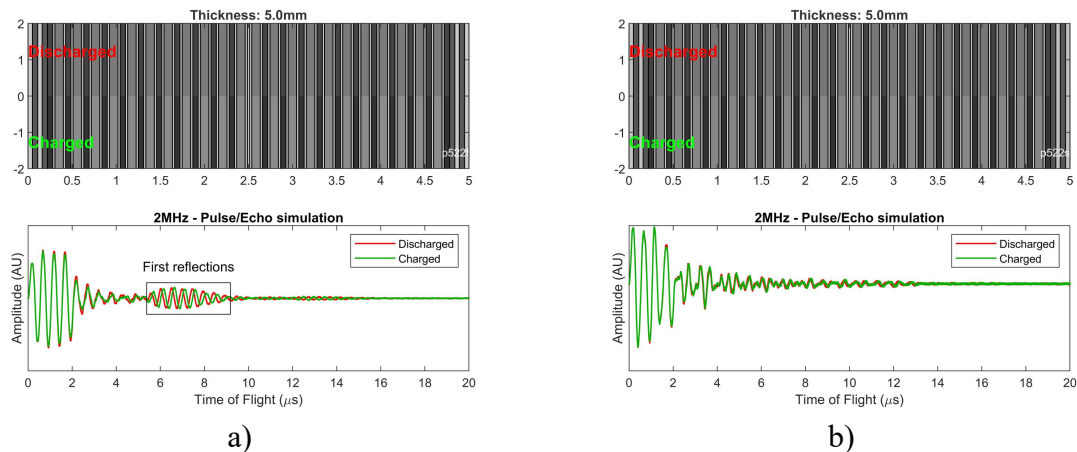


Figure 6: Model based on values taken from Table 1, separator wave speed for a) is 1128m/s and is altered to 685m/s in figure b) all other material properties and all dimensions remain the same for both models. This change creates a very different signal response as shown in the wave form.

Figure 6a illustrates the same model as that in Figure 5 with the grey scale representing the density/wave speed and relative thickness of each layer (top) and two A-scan responses (charged in green, discharged in red) overlaid (bottom). A box is drawn to show the region of the signal containing the ‘first reflections’. Figure 6b is the same model except for an arbitrary change in the separator material density (550kg/m^3 to 1450kg/m^3) which, once again holding the elastic modulus constant for this estimation, results in a change in separator wave speed of 1128m/s to 685m/s, all other parameters remain unaltered. Inspection of the bottom panel shows the change of separator property has a significant effect on the wave response. Two things are immediately clear resulting from this change, firstly, the change between charged and discharged states is greatly diminished in the right-hand model and secondly, the clear wave response has collapsed, there is no obvious region containing the first reflections and does not lend itself to taking an envelope from which to take readings.

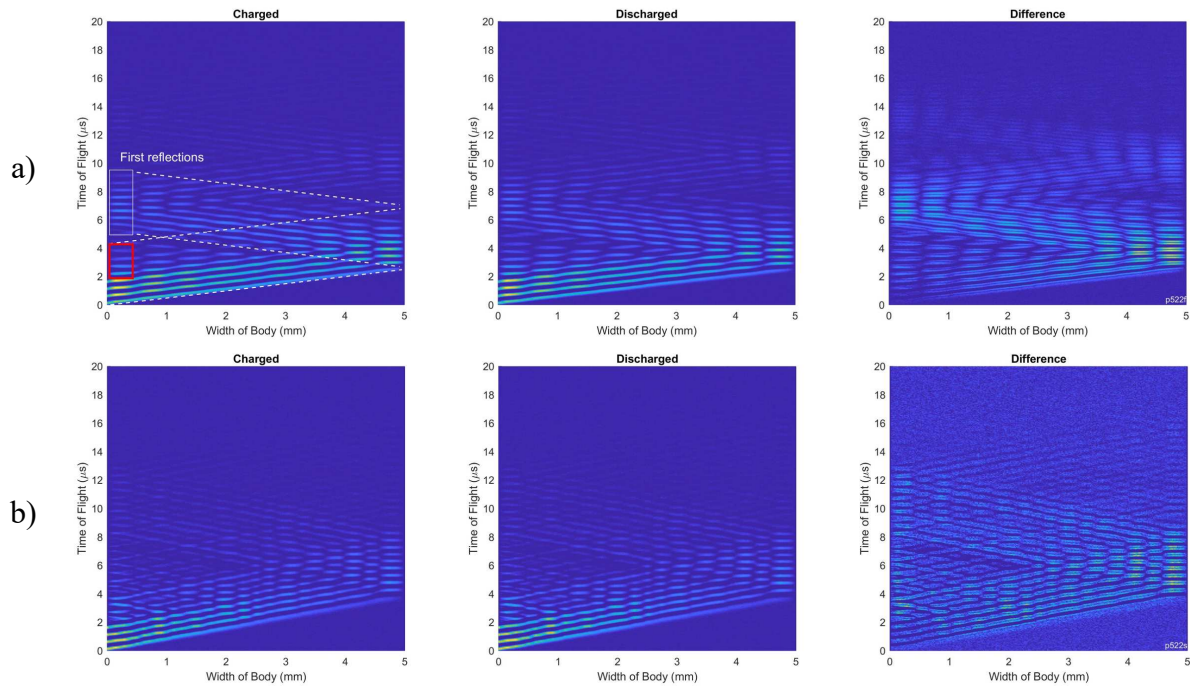


Figure 7: Waveform development, showing only wave peaks. For a) and b) Left-hand side is wave development for the charged state, centre panel shows the wave development for the discharged state and the right-hand side shows the absolute difference between the two charge extremes.

The panel of plots in Figure 7a show the historical wave development of the battery modelled in Figure 6a as it passes through the cell layers. This clearly shows a set of first reflections (highlighted in the white box) back to the sensor side of the battery cell (width = 0mm) which occurs between approximately $5\mu\text{s}$ and $8\mu\text{s}$. This region corresponds with the collection of peaks in the bottom panel of Figure 6a.

Observation of the difference panel (Figure 7a top right) confirms that these differences are driven by the incident waves (together with localised reflections and accumulated transmissions highlighted in the red box) reaching the opposing side of the body and returning the sensing edge of the cell. It can be assumed that waves of this nature collect and return information gathered through each layer of the cell twice (there and back) and would naturally be the most accurate to read.

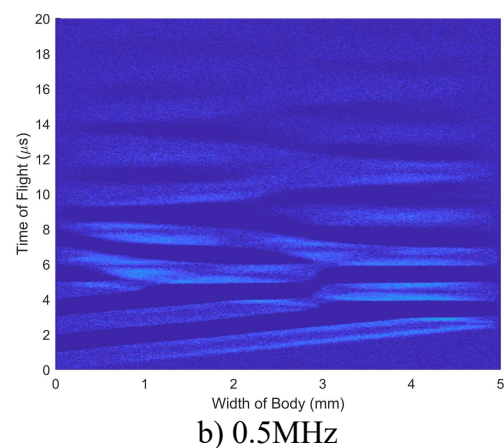
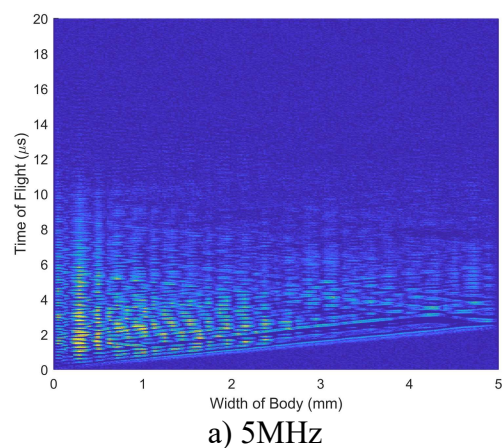
Using the model in this way demonstrates the complex interactions of transmissions and reflections that sum to form a particular waveform response. The change in separator properties cause the convenient first reflection group to break down (as shown in Figure 7b). Essentially the lower separator speed of sound causes a greater acoustic mismatch between separator and electrode and hence greater reflection at each interface (as shown in equation 2). The most intense regions in the differences plot are close to the first active layer encountered after the casing. This results in the signal struggling to penetrate the body causing a loss in battery measuring capability. In certain geometries, the signal can be dominated by reflections from large changes in material properties close to the sensor (casing materials/thickness) that will necessarily dominate the signal response. Locating a current collector can also have an effect as explored by Maier et al. ^[11], without knowing the precise construction of the cell it is difficult to ensure the signal response is optimised in terms of ultrasound correlation with SoC.

It would therefore be beneficial to have a method to identify the best waveform location to correlate with battery state of charge. To this end, experimental tests have been carried out with detailed analysis of the signal during different charge stages to explore methods of combating weak or unintuitive signal responses.

2.6. Confirming pulse frequency using model

During experiments, a pulse frequency of 1-2MHz was used, similar to the 2.25MHz used by Hsieh et al [6], this gave the clearest response and best battery charge correlations during testing. Using lower frequencies provided diminished changes in wave response, whereas higher frequencies produced more unpredictable signals with lower battery charge correlations. The effects of frequency choice can be visualised and the problems explained using model data.

Three frequency choices were 0.5MHz, 2MHz and 5MHz, all other parameters are held constant. The plots in Figure 8 show the absolute differences between the wave developments for both fully charged and discharged states. The higher amplitude, yellow regions are where there are highest discrepancies whilst dark blue shows low/no discrepancy. The development of the 5MHz wave collects some differences (Figure 8a), these are accumulated close to the initial pulse side of the cell, the differences fail to accumulate due to lack of cell penetration of the wave. As a result, the signal is dominated by layers close to the pulse/echo edge and are susceptible to temperature bias as this would include a high proportion of cell casing reflections. The 0.5MHz waves (Figure 8b) only detect minor changes as the wave lengths are considerably larger than the narrow layers they pass through, note a lack of wave development with yellow, high intensity changes. The 2MHz wave (Figure 8c) shows significant differences collect along the wave paths as they return to the sensing edge with a clear region of first reflections. This illustrates that 2MHz offers a good balance between cell penetration (lower frequency) and detail from layer reflections (higher frequency), providing solid theory behind the sensor/pulse selection process. Figure 8d shows the effect on the SoC correlations of the three frequency choices, the 2MHz performs well whilst the 0.5MHz and 5MHz register very weak/no useful battery charge correlation and are unsuitable in this instance.



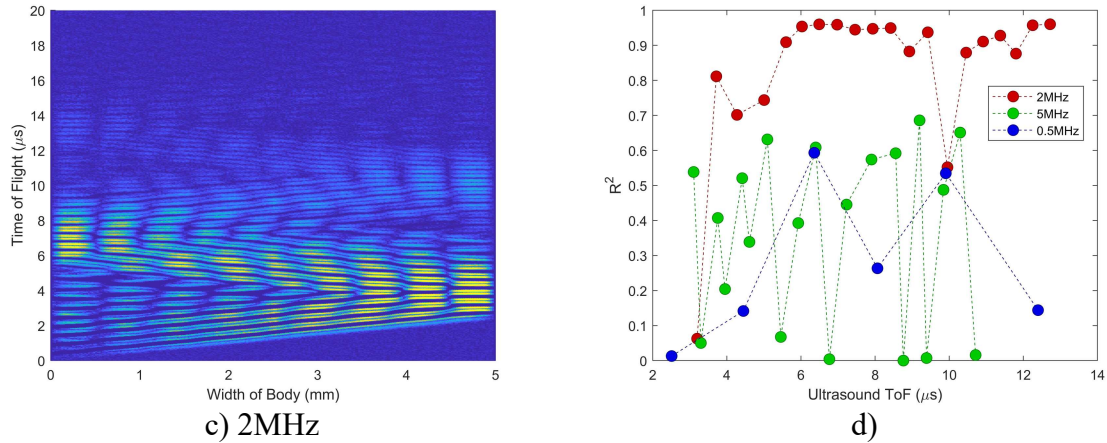


Figure 8: Charged/Discharged difference in ultrasound response plots. a) 5MHz shows small changes in wave development occurring close to initial pulses with lack of meaningful cell penetration. b) 0.5MHz wave passes through body almost unaffected by the changing properties in narrow layers. c) 2MHz passes through the cell with the incident waves gathering and accumulating changes, travelling back to the recording sensor side. d) Ultrasound ToF/battery charge correlation show 2MHz has strong relationship with battery SoC.

3. Experimental apparatus and instrumentation

The pouch cells used during testing were all commercially sourced lithium polymer rechargeable cells having a nominal voltage of 3.7V, a discharge/charge cut-off of 3.0V/4.2V and a capacity of 2Ah. The maximum discharge/charge current for the cells was 2000mA (1C)/1000mA (0.5C).

Commercial longitudinal contact transducers were used to both transmit and receive an ultrasound pulse in a pulse/echo arrangement as this is the simplest and most cost-effective method of capturing ultrasound data. The sensor was clamped in place and a high temperature ultrasound gel was used as couplant. The clamps were hand tightened enough to hold the sensor in place, minimum pressure was applied such that the sensor could be moved slightly while held in place. This was in to ensure no possibility of causing an accidental wave interface and in general care of the battery itself.

The sensor was connected to a PICOSCOPE 5000 Series oscilloscope which was used to generate the pulse and record the reflected waves. The pulse consisted of 2-3 sine waves at a frequency of generally 2MHz according to the discussion in section 2.6. The response signal captured ranged from 0-2 μ s to 12-30 μ s with a time resolution of 2-8ns. Signal captures were taken from every 60s to 300s depending on test length and each capture was recorded as the average of 20 captures taken at 20Hz.

Bespoke LabView software was used to control the PICOSCOPE in both signal generation and capturing the signal response. The software was also connected to a NI-9211 thermocouple input module to record the surface temperature of the cell during charge cycling. A schematic of test configuration is shown in Figure 9, cell images are shown in the top left corner. As the C-rates for the charge cycles were low and within the manufacturers stated maximums, no swelling occurred during testing and the cells remained in perfect physical condition throughout.

The battery was connected to a MACCOR 4000 Series Test System which controlled the charge cycling stages. Test were cycled according to a custom built programme generally

consisting of a combination of fixed current, fixed voltage and timed rest periods. In the fixed current stages, the rate of charge/discharge was generally 0.5C. The MACCOR records the battery voltage during charging and discharges up to 4.2V and discharges down to 3.0V, additionally, the Ah/s data is accumulated during cycling to provide a battery capacity profile, providing an alternative state of charge rating for the cell.

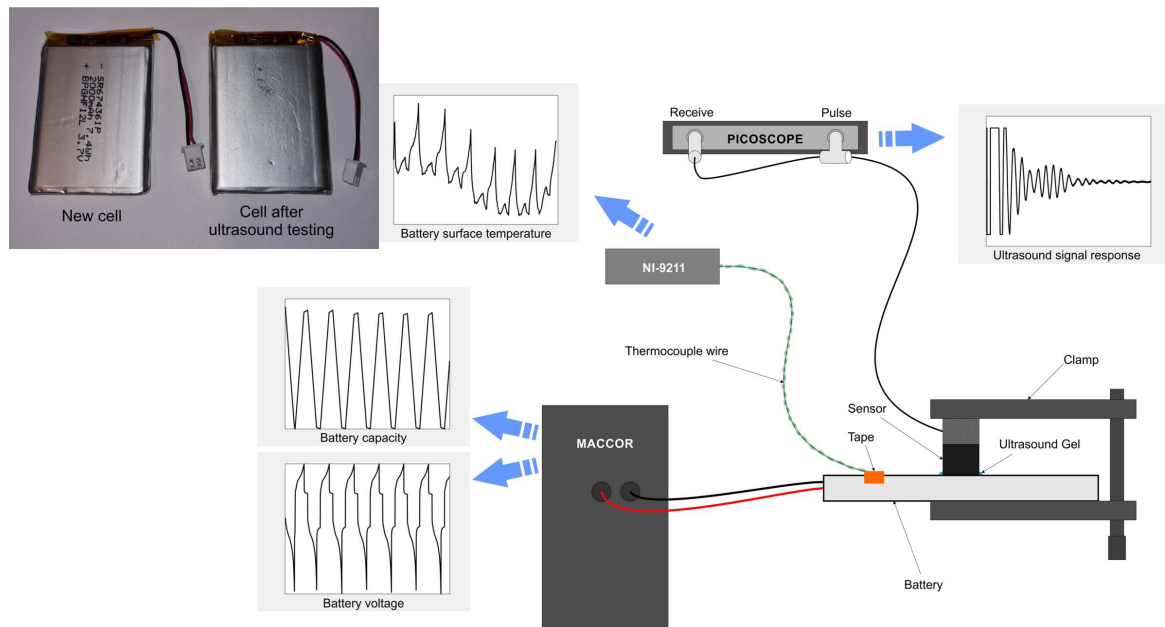


Figure 9: Test setup schematic

4. Analysis approach

Three data sets were retrieved (ultrasound response, charge data, surface temperature) during an experiment. The ultrasound data contains various information types, such as signal amplitude and time of flight changes which will vary based on which part of the signal a measurement is taken. Also signal power and frequency domain information is obtainable from the waveform. Additionally, the battery charge data provides voltage, current and capacity information. The analysis method developed was designed to incorporate all methods of data analysis such that the same data sets can be arranged in a variety of ways to assess the strongest correlations. There is also capability of tracking and measuring multiple signal peaks across the signal response to compare the results of each peak individually. The flow chart in Figure 10 shows these various methods of analysis available, the outputs of which will be discussed in detail.

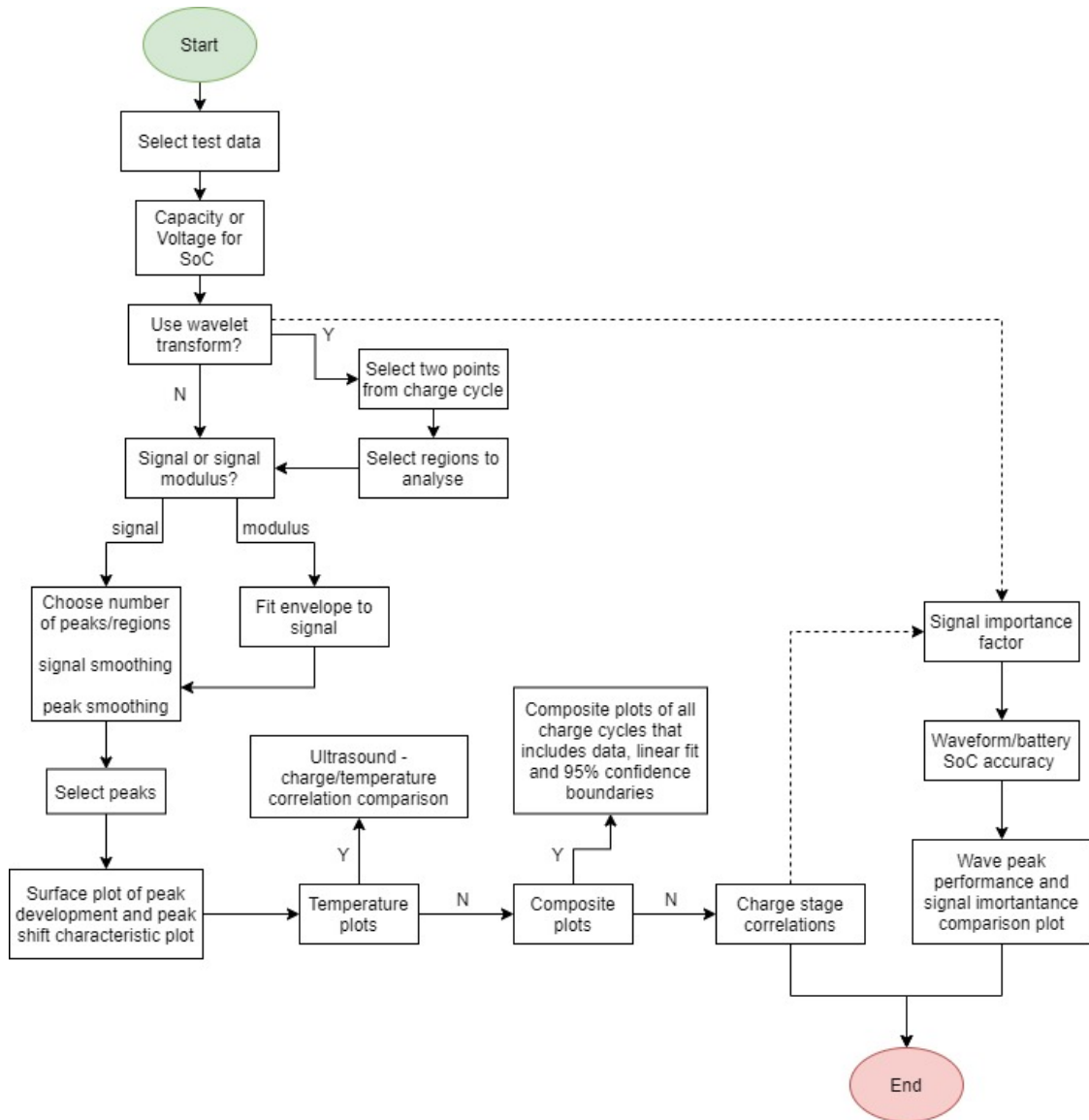


Figure 10: Analysis flow chart for analysis script created in MATLAB

The plots in Figure 11 show the initial formatting and data synchronisation process, the ultrasound and battery charge information is presented here with the peak tracking evident in Figure 11b. Note the tracking is colour coded to match the nature of the charge cycle which reveals a clear, significant and repeating pattern throughout the cycle stages. This peak tracking is a viable option for the automation of battery readings and therefore suitable for use in a battery management system.

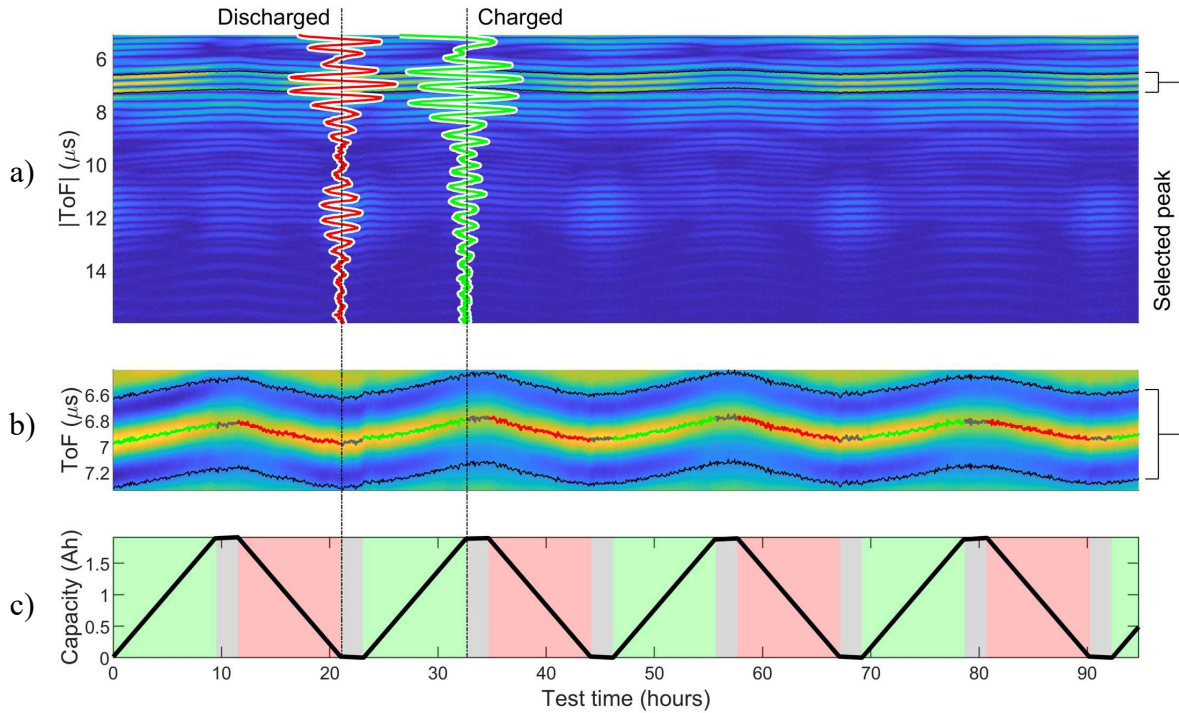


Figure 11: Measured ultrasonic amplitude intensity map as a battery is charged and discharged, each waveform (A-scan) is stacked (two sample signals shown, discharged state in red and charged state in green). The absolute values are shown in this plot for clearer viewing. The black solid lines show the area bounded by the user with a zoom of this in b) the peak is tracked throughout the test, each point is colour coded to identify the part of the charge cycle (green = charge, red = discharge, grey = rest), in c) The battery capacity is plotted over a colour coded background following the same colour coding. The black dashed vertical lines show the position of the two sample waveforms.

Some studies take measurements directly from the waveform and select a peak from which to take readings [11], [16], [17], most commonly, the largest peak found in the response. Popp et al. use a Schmitt-trigger method that captures a signal peak over a threshold and turns these into digital rectangular signals from which to measure [7] and signal power has been used as a means of capturing and quantifying ultrasound signal response [6]. Others have taken a readings from the peak of a signal envelope [14], [15]. This can often, but not always, correlate with battery state of charge, however obtaining an envelope that remains consistently strong across charge cycling is difficult to guarantee whereas selecting a peak directly from the signal is always possible. The problem with opting to measure from a single peak is being able to correctly identify the peak that carry battery charge insights. The following section compare the results of various measuring options to help identify a robust signal analysis strategy.

4.1. Waveform peak and peak envelope

Comparisons between measuring directly from a single peak and a signal envelope are shown in Figure 12, plots (c) and (e) relate the single peak selected in plot (a), and plots (d) and (f) relate to the envelope peak from the same signal in plot (b).

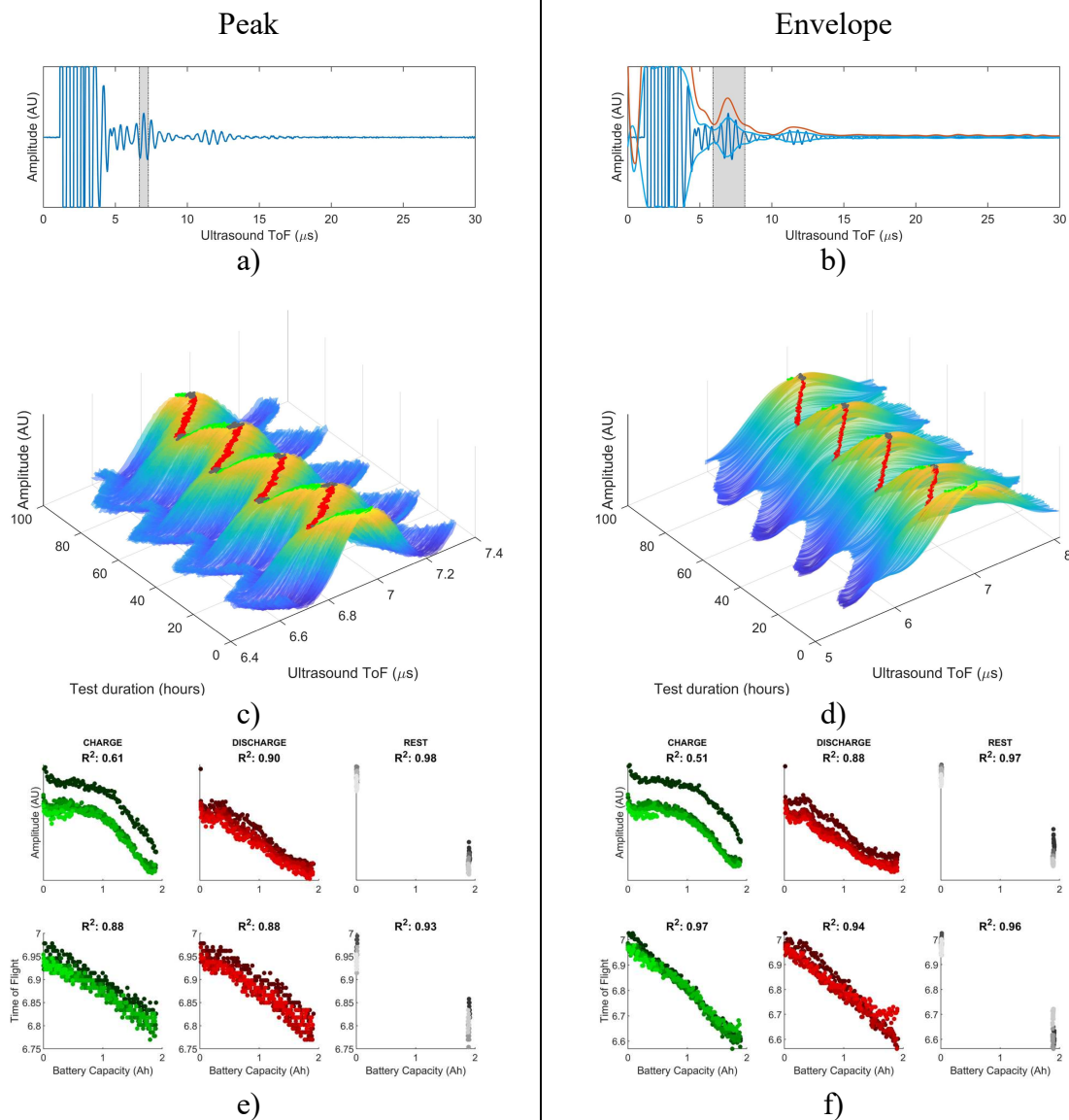


Figure 12: a) A single peak directly taken from the ultrasound response is selected and tracked throughout the test [step B in the flow chart Figure 7] b) the peak of an envelope can also be tracked in the same manner c) the graphical display of the peak evolution throughout the test [step C in the flow chart] d) graphical display for the envelope tracking e) separated correlation plots for charge/discharge/rest for the single peak for both signal amplitude (measured in arbitrary units) and time of flight [point D in flowchart] f) correlation plots for the envelope.

Peak tracking using either an individual peak or the envelope peak provides ability to take amplitude and time of flight measurements as the battery is charge cycled. The peak tracking is colour coded (red: charge, green: discharge, grey: rest) to highlight the battery charge status in Figure 12c and d. The change in time of flight and amplitude is recorded from this peak tracking throughout the duration of the charge cycling test, taken at the maximum point of the peak. Figure 12e and f, show correlation plots for the amplitude (top row) and time of flight (bottom row) measurements taken during charge cycling, the plots are also colour coded to show the different charge states according to the same scheme, with shaded points identifying data by its particular cycle.

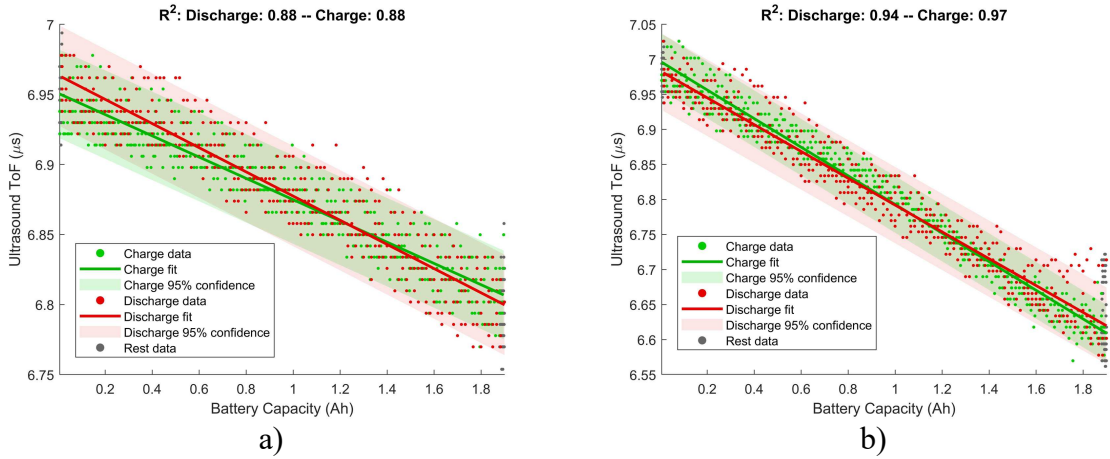


Figure 13: a) Using a selected peak directly from a waveform to monitor battery state of charge and b) using the peak of a waveform envelope [point A on flow chart].

The accuracy of each method typically depends on the signal and it is not obviously predictable which method will yield the best correlation. An envelope can help with signal to noise ratio and can perform some data smoothing effects. It can however combine the effects of the inaccurate parts of signal reducing the overall correlation with battery charge. In the composite plots in Figure 13, showing the same single peak and envelope analysis as in Figure 12, the signal envelope performs well and provides a slightly stronger R^2 value (~0.95) with battery state of charge than the single peak (~0.88).

In addition to the envelope not always providing the strongest charge correlations however, importantly, reliance of taking measurements from envelopes is problematic. As shown in the modelling, in some cases an envelope may be difficult to capture.

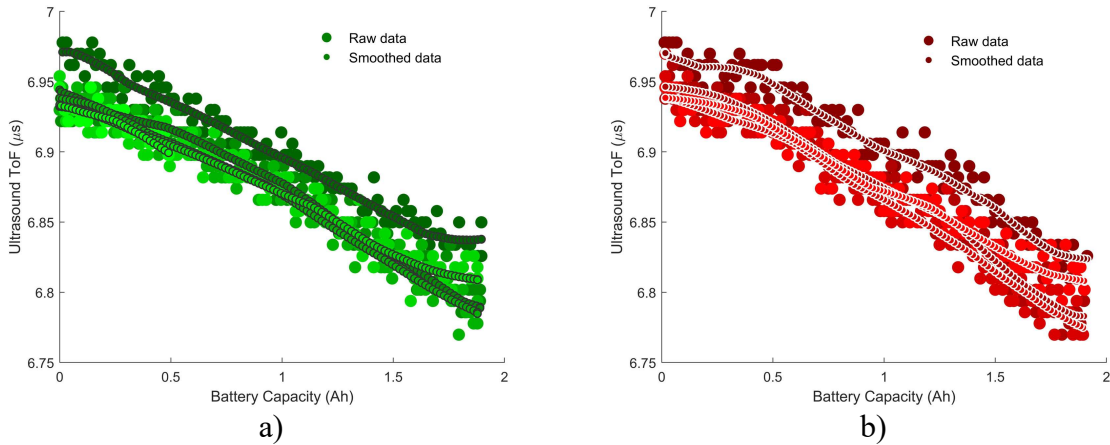


Figure 14: a) smoothed charging data b) smoothed discharging data

A note on the accuracy of the data. As this study is concerned with the quality of different peaks within the signal rather the quality of signal itself, raw captured data is shown throughout. There are several means of improving data accuracy however, denoising can be performed in data processing, the data in Figure 14 has been denoised using a *sym4* wavelet twice, firstly the selected peak is smoothed to aid peak tracking accuracy, following from this the peak tracking itself is denoised, along both the ToF and amplitude axes. The results are overlaid, this simple measure both improves the precision of the relationship between US and

SoC and gives some further context to results, an isolated cycle becomes clear, likely due to a temperature change.

Data acquisition improvements can also be made, such as increasing the capture rate from 20Hz or increasing the pulse voltage to improve signal to noise ratio. There are several alternative methods of arranging sensors as discussed previously and whilst many of these studies aim to improve signal accuracy with respect to battery information, this study is focused on the qualities within the signal itself.

4.2. Battery voltage or battery capacity to define state of charge

Most current literature uses voltage as the measure of battery state of charge for ultrasound comparisons, with a few exceptions that used battery capacity [7], [15], [18]. This analysis will compare both. Figure 15 shows that ultrasound has a much stronger relationship with the battery capacity than with the voltage. Two points are important to note; firstly, tracking battery capacity with ultrasound gives a much stronger R^2 value (~ 0.89) average compared to (~ 0.64) for voltage, this is evident in the voltage plot where a clear linear relationship is absent. Secondly, the changes for charge and discharge occur in a similar fashion when tracking capacity with ultrasound. The changes occur at different voltage ranges, this lack of similarity between charge and discharge would make taking readings much more difficult.

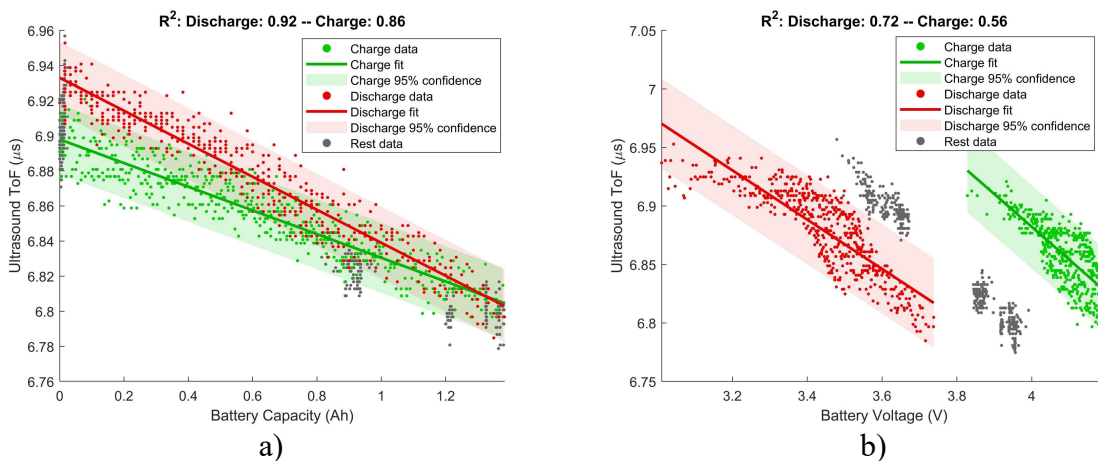


Figure 15: a) Using battery capacity as the measure of battery state of charge and b) using battery voltage as a measure of state of charge. [These plots are from point A of the analysis flow chart]. Note that these results were taken from a quick charge, as a result the voltage jumped straight to just over 3.8V when charging after resting and just under 3.8V when discharging after resting, notice the reduced capacity as a results (1.3Ah)

4.3. Measurement from signal amplitude or time of flight

As previously mentioned, published studies used signal amplitude and time of flight shift to monitor ultrasound changes for battery measuring purposes. In Figure 16a, a clear linear relationship between battery capacity and ultrasound time of flight is visible. The same relationship is much less clear for peak amplitude (Figure 16b), especially for the charge part of the cycle which has a R^2 value of only 0.01, being non-linear and complicated to measure.

Figure 16c shows the correlations for capacity and temperature against change in ToF and signal amplitude across the whole signal, with the selected peak measured in Figure 16a and Figure 16b highlighted in grey. Notice that the capacity/ToF (blue circles) and

temperature/amplitude (orange squares) correlations are higher, whilst the capacity/amplitude (blue squares) and temperature/ToF (orange circles) have little to no correlation anywhere in the signal. The highest correlation in this test is the capacity/ToF at the selected peak. Signal peak amplitude can occasionally provide good capacity measurements but being sensitive to temperature changes makes it an erratic and unreliable indicator of battery charge, this is discussed in section 5.2.

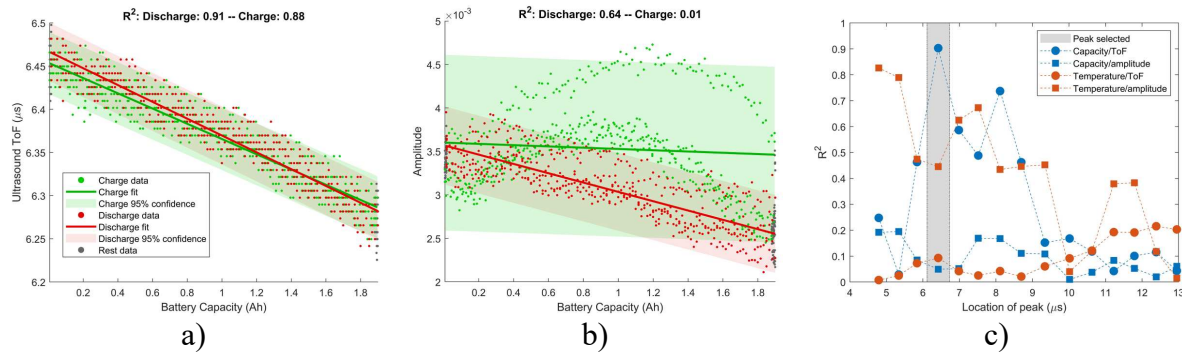


Figure 16: Composite plots with linear fit details, a) time of flight from a single peak measurement and b) signal amplitude from the same single peak measurement. c) the location of the peak displayed in a) and b) with measurement correlations from across the signal for comparison, averaged using next peak data for clearer viewing.

4.4. Difficulties obtaining signal envelope

As mentioned previously, in some experiments, it is difficult to identify suitable envelopes from which to take readings (example shown in Figure 17a). From the model in Figure 6 it was shown that, apart from being an instrumentation issue, flattened signal could result from the specific nature of the layered properties in the battery, this could typically be caused by some significant interface boundary along the wave path rendering the incident wave unable to return back to the sensor with clarity (e.g. casing, gas build-up, current collector, large layer acoustic mismatch). It is important to note that this is not a signal to noise issue and increasing the pulse voltage will merely increase the whole signal, including reflections. The linear fit plots in Figure 17b and c show the problems when deciding from which part of the signal measurements should be taken. Peak #1 is taken where there is a large defined peak available having decent signal to noise ratio and at around 6µs should contain some of the first reflections when comparing with the model and other experimental results. Peak #2 is from much later in the waveform that has suffered significant attenuation with a poorly defined peak. However, peak #1 shows little relationship with the battery capacity, whereas peak #2 has a good correlation. Whilst the R² values are not as strong as in other tests, it remains a valuable exercise to identify a suitable method that would maximise the battery information should a signal such as this be obtained.

Note this test contained a constant voltage section in the charge cycling, this is denoted in the peak tracking using a blue line. The blue line shows that the ultrasound peak continues to develop along a similar trajectory to the green (charge) line, until the grey (rest) period is reached. The linear fit for this data confirms the relationship is an extension of the charge data albeit at a different rate which would be expected as the current gradually decreases approaching capacity.

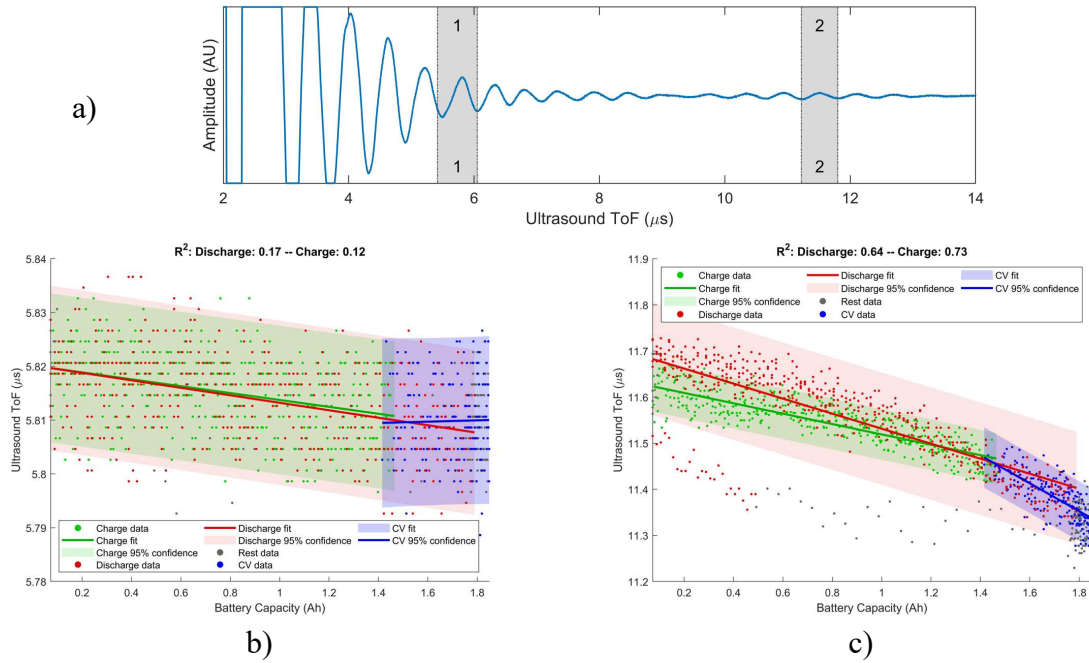


Figure 17: a) Experimental test signal response. Not suitable for taking an envelope, two peaks tracked for battery state of charge accuracy. Linear fit for peak #1 shown in b) and linear fit for peak #2 shown in c)

4.5. Temperature effect on ultrasound signal

The speed of sound of materials varies with temperature and since battery temperature fluctuates during charge cycling it needs to be considered. In Figure 18a, battery temperature is synchronised with the charge cycling data and the clear repeated effect of charge on cell temperature is evident. The laboratory ambient temperature is also seen to have an effect altering the underline baseline temperature.

Figure 18b shows the correlation between change in ultrasound ToF for each individual peak in the signal response and battery capacity/battery surface temperature. This clearly shows a greater relationship between US and SoC when compared to US and temperature. There is a very strong relationship at 6-9 μ s with SoC whilst the temperature shows no relationship until a switch in correlation occurs late in the signal.

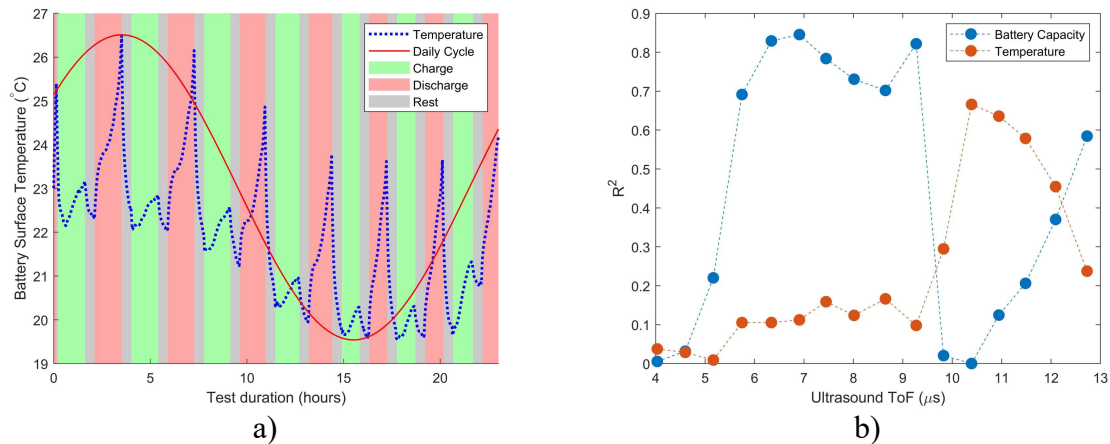


Figure 18: a) Battery surface temperature variation recorded during testing. The coloured bars behind the plot denote the stage of charge cycling (charge/rest/discharge/rest). The red line shows the daily cycle in which a maximum and

minimum ambient temperature affects the base line. b) Ultrasound/battery capacity and ultrasound/battery surface temperature correlations shown across the length of an ultrasound response. [step H on flow chart]

Changes in global wave speeds are built into the model to simulate cell temperature changes, two examples are shown in Figure 19. In model a) the temperature gain is set to 5°C during cycling, this occurs both as a combination of ambient cycling temperature and in accordance with the charge cycle. This shows similar results to the experimental data, the correlation is strongest with battery charge. In model b) the temperature gain is increased to 25°C and this results in a reduction in battery charge/US correlation and an increase in temperature/US correlation. This suggests that significant temperature increases, either ambient or internally driven, will limit the charge measurement capability of the ultrasound signal.

A strong signal with good cell penetration contains good battery density change and therefore battery charge data. Locating this region when taking measurements is vital, parts where the incident wave is traveling through the cell and is away from the sensor edge (for example 0-4 μ s and 10-12 μ s in the waveform development plot in Figure 7a) show the signal to have weak correlation with battery charge. This is shown in both the experimental data in Figure 18b and in the model data in Figure 19a. In both cases, where charge correlations diminish, temperature correlations increase. Here, signal peaks contain accumulations of shallow wave penetrations largely influenced by the casing materials where changes in wave speed can only be attributed to temperature changes.

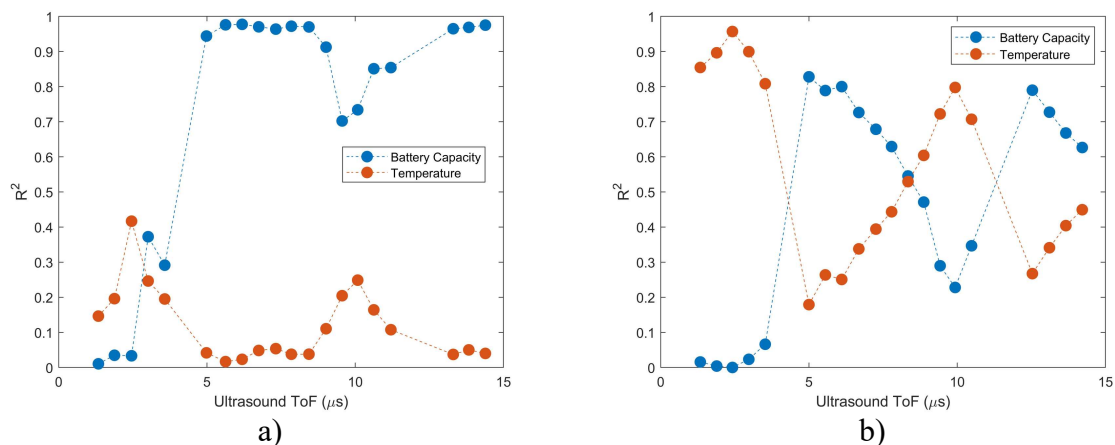


Figure 19: Battery capacity/temperature – ultrasound correlation plots a) 5°C gain during charge cycling and b) 25°C gain during cycling. The model increases the global wave speed 1.0m/s for each °C increase.

5. Adaptive peak tracking for battery cell variation

5.1. Cross wavelet transform

In the current literature, analysis has almost exclusively focused on ultrasound signals in the time domain, with little regarding the effects of battery changes on the signal in the frequency domain. Gold et al, compare wavelengths of the second compressional wave to the charge of the battery which showed wavelength and amplitude were a function of charge [15]. Apart from this all studies focus on the signal power (the area under the curve of the signal), peak amplitude, or peak time of flight change.

Various methods are tried here to identify if information from the frequency domain can aid in determining parts of the waveform that have strongest correlations with change in battery capacity. A fast Fourier transform (FFT) will provide signal information in the frequency domain at the expense of losing all time-based information. The short-time Fourier transform (STFT) technique is a time-frequency analysis and can help identify not only changes in frequency but also where in the time domain these changes occur. This method has been previously used in attempts to detect acoustic echoes embedded in a signal response through layered bodies^[19]. The STFT method suffers from a necessary compromise between good time/frequency resolution. A method that somewhat eliminates this time/frequency accuracy trade-off is a continuous wavelet transform (CWT) which has also been used to detect echoes in multilayered structures^[20].

Experimental data time/frequency plots transformed using a CWT are shown in Figure 20a (charged) and Figure 20b (discharged). These plots show the amplitude across the frequency spectrum (y-axis) along the waveform duration (x-axis), with yellow being high amplitude and blue being low amplitude. Activity is observed across a broad range of frequencies, with concentration around a 2MHz frequency band by around 6 μ s before attenuating by approximately 10 μ s, this region would be expected to be the location of the first reflections. The greyed regions denote the cone of influence (COI), a feature of wavelet transforms that causes lower frequency bands to have increased edge effects and must be disregarded.

The battery ultrasound measurements rely on change in signal (ToF/amplitude) rather than an absolute measurement value (i.e. variation in ultrasonic response are observed as a battery feature, such as charge changes). As such, a useful tool to use to monitor these changes in the time/frequency domain is the cross wavelet transform (XWT). This method was developed by Grinsted et al, originally to monitor the Arctic oscillation being a key aspect of climate variance in the Northern Hemisphere^[21], but can be applied to any two sets of time series data. A XWT plot is shown in Figure 20c, regions in the time/frequency domain that share high common signal power properties are denoted as high intensity (yellow), the arrows show the phase changes with right arrows showing in-phase, left arrows anti-phase, down arrows charge lead discharged by 90°. The black border surrounding certain parts of the plots denoted regions with 5% significance against noise, a feature which is not used in this analysis. The COI is again rendered on the plot showing regions at lower frequencies where insights are to be disregarded.

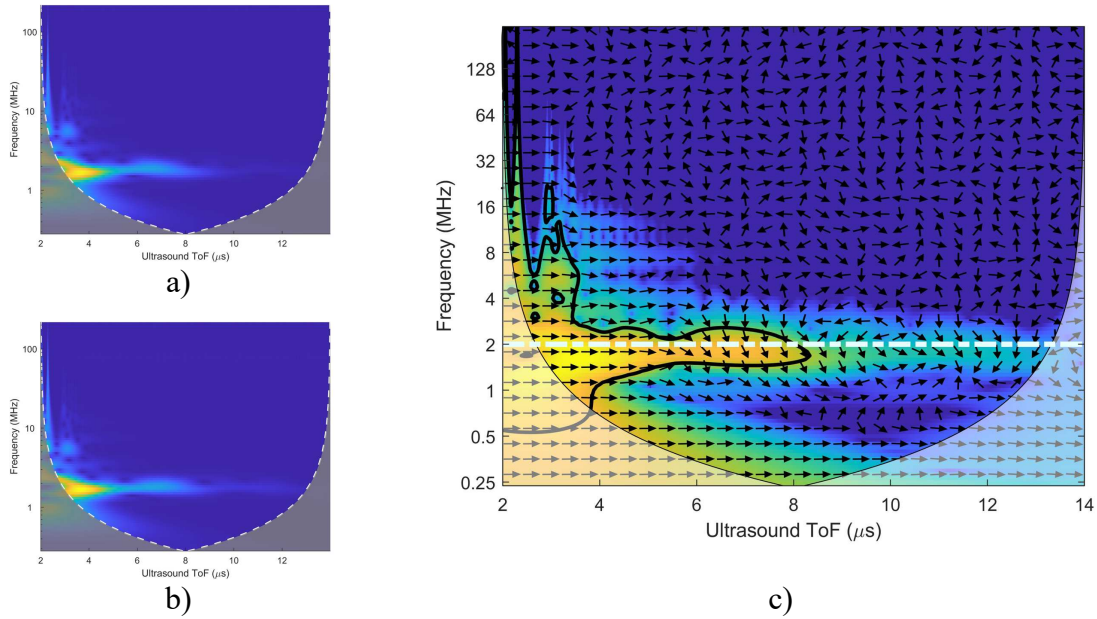


Figure 20: a) Continuous wavelet transform (CWT) for the signal when the battery is charged, and b) discharged, c) cross wavelet transform (XWT) showing frequency bands where both signals have strong similarities in amplitude shown in the higher (yellow) intensity regions, arrows mark the phase shift between the signals [arrow right: in phase, left: anti-phase, down: charged leading discharged by 90°] [21]

From the XWT shown in Figure 20c, a parameter for determining the most accurate part of the signal from which to take battery charge readings can be obtained. It can be safely assumed that the pulsing frequency is a known value and as such that frequency can be isolated (shown by the dotted white line at 2MHz in Figure 20c). Taking the intensity value along this line gives the XWT amplitude plot shown in Figure 21a. This is normalised between 0 and 1 and has a large peak at the beginning of the signal at around $3\mu\text{s}$. This peak corresponds to the incident pulse and would be of no practical use. There is however a second peak between 6 and $7\mu\text{s}$. The phase shift value in Figure 21b captures the phase change which is also normalised between 0 and 1. Here it can be seen that there is little or no shift in phase until around $6\mu\text{s}$ and then there are fluctuations across the selected frequency after this, growing in intensity and erraticism. In Figure 21c, there is an arbitrary, exponential function, providing weighting towards later parts of the signal. The weighting is constructed based on the assumption that later peaks in the signal have travelled further, will include more reflections and therefore hold greater battery insights. This additional parameter also serves the purpose of eliminating or deemphasizing the very early parts of the signal (potentially shallow signal depth penetration, dominated by early layer echoes and often prone to transducer ringdown effects). Finally, in Figure 21d, the three values are multiplied to provide a signal importance variable. The variable can guide and potentially automate, based on comparing two signal captures, where to measure peaks to optimise the accuracy of battery charge information. It is important to note that this method works from any two, non-identical, wave captures taken whilst charge cycling. In Figure 21a-d the dashed lines represent the arbitrary partial charge points marked in grey in Figure 21e. Although the intensity of the signal importance factor is lower, the identification of the most important section of the signal remains clear and accurate.

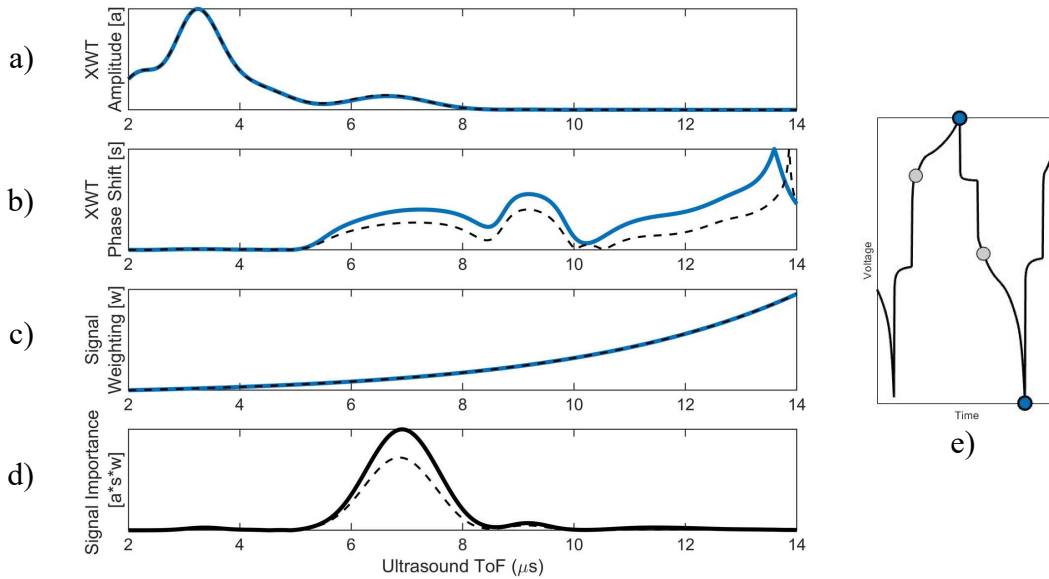


Figure 21: Signal importance factor calculation [point E on the flow chart]. Solid lines represent reference taken at charge extremes (blue markers in plot e), dashed lines from reference taken at arbitrary partial charge points (grey markers in plot e).

5.2. Smart peak selection

Using the XWT to define the signal importance factor enables identification of waveform regions that maximise two conditions; (i) good signal amplitude when at both extremes (or any two non-identical parts) of the charge cycle and (ii) have significant phase shift activity.

In Figure 22 the smart peak selection region is shown as peaks on the black line (signal importance factor); this shows a clear maximum between 6 and 8 μs . By plotting the time of flight/battery charge correlations (blue line) and the signal amplitude/battery charge correlations (pink line) two points become quite clear. Firstly, the smart peak selection region identifies the waveform region that best correlates with battery charge data and the variation for both charged and discharged states is low (narrow band on the shaded region). Secondly, it confirms that time of flight, rather than amplitude, is a more stable measure to gain battery SoC insights.

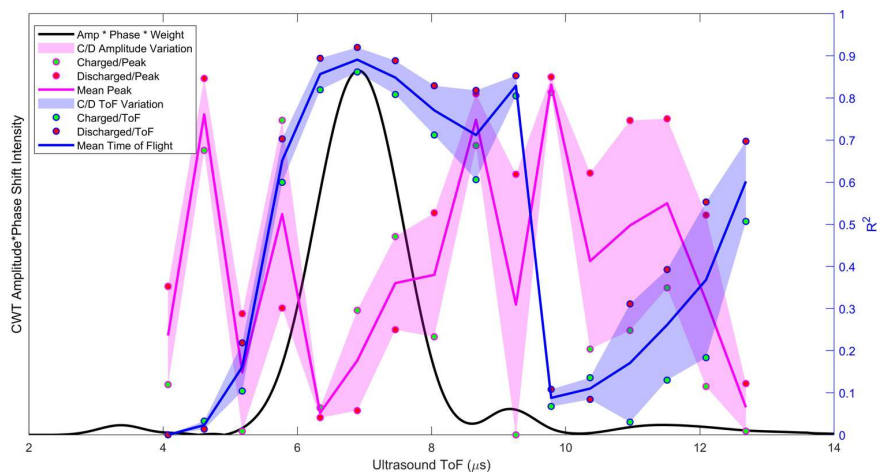


Figure 22: Smart peak selection method of locating best region for taking battery measurements [step F on flow chart]. Signal peak amplitude-ToF/battery SoC correlation across the waveform.

Figure 23 shows an ultrasound response waveform marked up with all the strategies to suggest from which region to extract measurements. The signal itself is drawn with the regions suggested as containing best battery correlations in a thick black line, the signal is faint and thin elsewhere. Each peak selected for analysis has a marker, the size of which represent the strength of correlation with battery state of charge. The deepness of red is used to indicate the discrepancies in correlations between charge and discharge parts of the cycle. This smart peak selection should show large, deep red markers on the peaks of the signal shown drawn with thick black lines. A useful feature of this method of peak selection is that as the XWT amplitude variable detects regions where both signals share high common power, disappearing peaks of interest are automatically filtered out. This helps to guard automatically against unstable recordings.

The point on the peak at around $7\mu\text{s}$ is large and deep red. This can be seen in Figure 22, where the ToF/battery capacity R^2 values during both charging and discharging are 0.86 and 0.92 respectively. The point at the peak at around $11\mu\text{s}$ is small and almost white, this can be seen in Figure 22 where the ToF/battery capacity R^2 values whilst charging and discharging are 0.03 and 0.31 respectively and would be unsuitable for battery monitoring purposes.

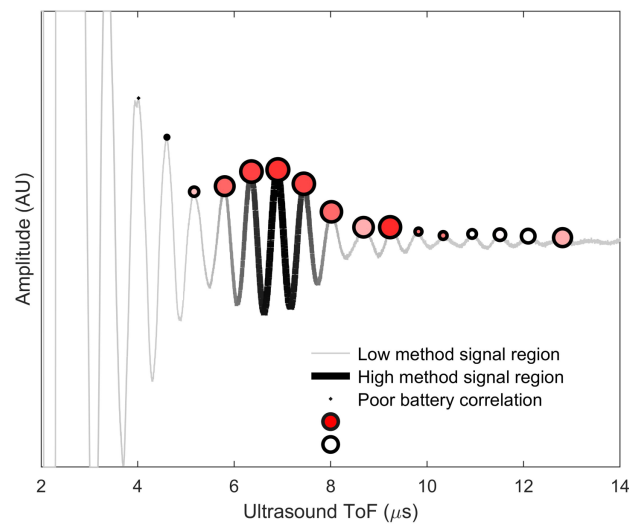


Figure 23: Smart peak selection waveform mark up. The ultrasound response waveform is displayed with thick black lines to denote regions of signal that are favoured by the smart peak selection method. The size of the point at each peak represent the strength of correlation with battery state of charge (large points are best) and the deepness of the red in those points shows the variance between charge and discharge parts of the cycle (deep red is best). [step G on the flow chart]

Many signals produce a noticeable collection of peaks that represent the first reflection waves that have travelled there and back through the battery. This is an intuitive place to take measurements from and are appropriate to capture signal envelopes, however some signal responses do not provide this. The signals in Figure 24 are taken from batteries of the same specification and manufacture as previous using identical test equipment and methodology. The signal in Figure 24a is difficult to envelope and gain a defined peak from which to take measurements. However, here are a collection of peaks that would appear suitable for taking

charge measurements. The signal drawn in thick black between 13 and 15 μ s contains two or three peaks that have strong correlation and low charge/discharge variance.

The signal in Figure 24b is lower quality and no obvious peaks are evident with a good signal to noise ratio as good candidates for taking charge measurements. The smart peak method in this case highlights very early (3 to 5 μ s) signal and these peaks provide poor battery information (the sound wave has not travelled through the cell layers and there appears to some transducer ring down). The second, shorter group of smart selected peaks from 11 to 12 μ s reveal the region that contains peaks containing best battery charge correlations. Recall from the modelling data, that early signal is usually dominated by casing and suffers from lack of cell penetration and should be avoided, the second shallow peak would be preferable.

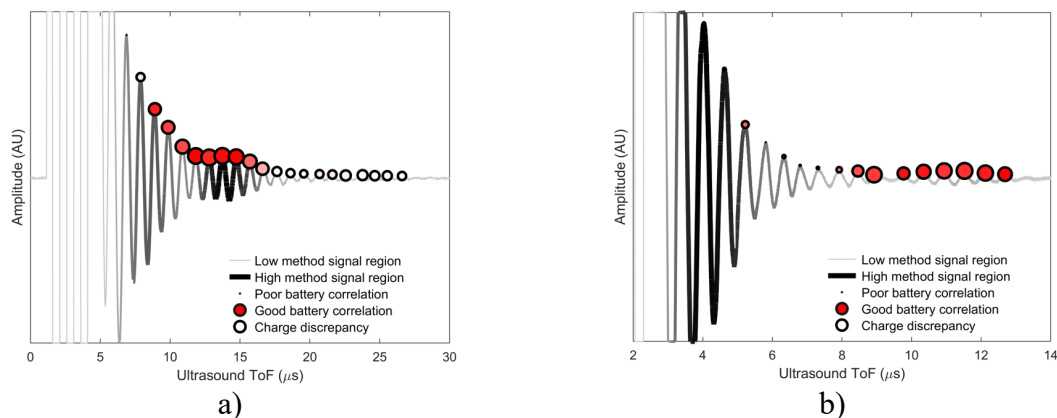


Figure 24: a) Signal that is difficult to provide a consistent peak of an envelope, smart peak selection shows that peaks drawn in thick black lines have the strongest battery charge correlations and are most consistent across charge/discharge parts of the cycle. b) This signal has little scope for enveloping, no obvious peak as a candidate for taking measurements, first smart peak region inaccurate, second more shallow region successfully locates peaks with best battery charge correlations.

6. Discussion – Practical implementation

Ultrasound measurements would likely be used in conjunction with traditional battery measuring methods, such as voltage readings, to enhance the accuracy of charge estimations. The smart peak selection method can help optimise and protect ultrasonic battery measurements, particularly where the signal response is weak or contains unexpected features. Causes of these problems could include variations in battery geometries and sensor instrumentation.

This method of battery monitoring is a practical means of gaining true insights into the internal changes occurring during battery charge cycling. Although this work utilised commercial contact probes to gain ultrasound readings, much smaller instrumentation methods are possible. For example, discs or cut piezoelectrical plates, low profile and size order of a few mm's requiring very thin wiring. To ensure responses with good cell penetration additional factors such as adhesion and damping must be considered, this would still allow for a very small and cheap instrumentation set up. Results can be obtained using a single sensor, keeping materials to the minimum required for this method and only one face needs to be accessible. Pulsing/receiving circuits are also small and inexpensive, of the order of £10s, and with the application of pulse sequencing tables, could control the pulse, signal

capture and data processing of all connected battery cells. All the experimental data analysis performed in this study, including peak tracking and smart peak selection requires minimal processing time and power and is suitable for live monitoring purposes. Any improvements in the accuracy of ultrasound data acquisition would improve the accuracy of methods covered in this study.

7. Conclusion

This study examines the reflection of an ultrasound pulse travelling through layers in a battery cell, and how that signal responds to battery state of charge changes. Reflections occur at each interface within the battery structure and the composite reflected signal consists of many peaks. Early peaks tend to be larger, but the responsible wave has not travelled through all the battery and so contains less information about the structural changes (such as the change in properties caused by lithium uptake during charging).

A model was created based on the wave equation PDE. From this model it is revealed how small changes to the properties of the battery layers can have significant effects on the characteristics of the ultrasound response signal. Dimensional, density or ordering changes from battery to battery can cause the signal to vary in each case, this can impair the intensity of wave changes as a function of state of charge and could render envelopes difficult to obtain should that be the method of measurement.

From analysis of experimental data, it was shown that battery ultrasound response has a much stronger correlation with battery capacity than with battery voltage. In fact, the relationship between ultrasound and capacity is linear which confirms the ultrasound is detecting density changes during cycling as lithium passes between anode and cathode. Some studies opt to take readings from a signal envelope, this study finds that this method does not provide consistent advantages over a single peak from the signal and as an envelope is not always guaranteed to be available, individual peak selection is the safest option.

Signal peak amplitude and change in time of flight do not alter with SoC in the same manner, it is shown that time of flight has stable correlations with battery charging whereas although some peaks have good amplitude/charge correlations, this is much more erratic across the signal. For this reason, time of flight is regarded as the best method for gaining a single measurement for battery state of charge. This is confirmed in tests including constant voltage sections of charge cycling. The time of flight will continue to change along the same path as the constant current charge section. However, the rate of change is altered, reflecting the rate of change in capacity level.

Change in temperature is a factor that affects wave speed through any medium, along with changes in density and elasticity. To assess the effect of temperature, a thermocouple was attached to the battery during cycling, it was found that both battery activity and the ambient temperature of the laboratory caused changes in battery surface temperature by $\pm 7^{\circ}\text{C}$ and this has little effect on the stability of the time of flight readings. From the model however, it was shown that should the temperature effects be large enough this could prevent the capability of taking reliable and accurate ultrasound/SoC readings.

Selecting the correct peak from which to take time of flight measurements is not trivial and the obvious and intuitive peak may not provide any useful battery information. A method using the cross wavelet transform to gain amplitude and phase shift activity along the

transducer/pulsing frequency band across the signal, can provide a 'smart peak' selection region that has the capability to automate the peak that will provide the most accurate battery charge measurements. This method relies on two reference signals from non-identical parts of the charge cycle to be effective.

8. Acknowledgments

The authors would like to acknowledge the financial support of Ricardo Ltd and the advice and guidance of Prof Jon Wheals, Michael Wheeldon and Dr Henry Dodson. RDJ would like to acknowledge the Engineering and Physical Sciences Research Council for funding this research through his fellowship on *Tribo-Acoustic Sensors* EP/N016483/1 and the Centre for Doctoral Training in Integrated Tribology EP/L01629X/1.

9. Declaration of Interest Statement

There were no conflicts of interest.

10. References

- [1] V. Ramadesigan, P. W. C. Northrop, S. De, S. Santhanagopalan, R. D. Braatz, and V. R. Subramanian, "Modeling and Simulation of Lithium-Ion Batteries from a Systems Engineering Perspective," *J. Electrochem. Soc.*, vol. 159, no. 3, pp. R31–R45, Jan. 2012.
- [2] L. Lu, X. Han, J. Li, J. Hua, and M. Ouyang, "A review on the key issues for lithium-ion battery management in electric vehicles," *J. Power Sources*, vol. 226, pp. 272–288, 2013.
- [3] J. Wen, Y. Yu, and C. Chen, "A Review on Lithium-Ion Batteries Safety Issues: Existing Problems and Possible Solutions," *Mater. Express*, vol. 2, no. 3, pp. 197–212, Sep. 2012.
- [4] G. O. Sahinoglu, M. Pajovic, Z. Sahinoglu, Y. Wang, P. V. Orlik, and T. Wada, "Battery State-of-Charge Estimation Based on Regular/Recurrent Gaussian Process Regression," *IEEE Trans. Ind. Electron.*, vol. 65, no. 5, pp. 4311–4321, May 2018.
- [5] Y. Zheng, M. Ouyang, X. Han, L. Lu, and J. Li, "Investigating the error sources of the online state of charge estimation methods for lithium-ion batteries in electric vehicles," *Journal of Power Sources*, vol. 377. Elsevier, pp. 161–188, 15-Feb-2018.
- [6] A. G. Hsieh *et al.*, "Electrochemical-acoustic time of flight: in operando correlation of physical dynamics with battery charge and health," *Energy Environ. Sci.*, vol. 8, no. 5, pp. 1569–1577, 2015.
- [7] H. Popp, M. Koller, S. Keller, G. Glanz, R. Klambauer, and A. Bergmann, "State Estimation Approach of Lithium-Ion Batteries by Simplified Ultrasonic Time-of-Flight Measurement," *IEEE Access*, vol. 7, pp. 170992–171000, 2019.
- [8] G. Davies *et al.*, "State of Charge and State of Health Estimation Using Electrochemical Acoustic Time of Flight Analysis," *J. Electrochem. Soc.*, vol. 164, no. 12, pp. A2746–A2755, 2017.
- [9] C. Bommier *et al.*, "Operando Acoustic Monitoring of SEI Formation and Long-Term Cycling in NMC/SiGr Composite Pouch Cells," *J. Electrochem. Soc.*, vol. 167, no. 2, p. 020517, 2020.
- [10] B. Sood, M. Osterman, and M. Pecht, "Health Monitoring of Lithium-ion Batteries," *2013 IEEE Symp. Prod. Compliance Eng.*, pp. 3–8, 2013.
- [11] M. Maier, T. Compton, J. B. Robinson, D. J. L. Brett, G. Alster, and P. R. Shearing, "Spatially resolved ultrasound diagnostics of Li-ion battery electrodes," *Phys. Chem.*

- Chem. Phys.*, 2018.
- [12] J. Krautkrämer and H. Krautkrämer, *Applied Ultrasonic Testing of Materials*. 1969.
 - [13] R. S. Dwyer-Joyce, “The application of ultrasonic NDT techniques in tribology,” *Proc. Inst. Mech. Eng. Part J J. Eng. Tribol.*, vol. 219, no. 5, pp. 347–366, 2005.
 - [14] P. Ladpli, F. Kopsaftopoulos, and F. K. Chang, “Estimating state of charge and health of lithium-ion batteries with guided waves using built-in piezoelectric sensors/actuators,” *J. Power Sources*, vol. 384, no. February, pp. 342–354, 2018.
 - [15] L. Gold *et al.*, “Probing lithium-ion batteries’ state-of-charge using ultrasonic transmission – Concept and laboratory testing,” *J. Power Sources*, vol. 343, pp. 536–544, 2017.
 - [16] J. B. Robinson, M. Pham, M. D. R. Kok, T. M. M. Heenan, D. J. L. Brett, and P. R. Shearing, “Examining the Cycling Behaviour of Li-Ion Batteries Using Ultrasonic Time-of-Flight Measurements,” *J. Power Sources*, vol. 444, no. September, p. 227318, 2019.
 - [17] Y. Wu, Y. Wang, W. K. C. Yung, and M. Pecht, “Ultrasonic Health Monitoring of Lithium-Ion Batteries,” *Electronics*, vol. 8, no. 7, p. 751, 2019.
 - [18] W. Chang, C. Bommier, T. Fair, J. Yeung, S. Patil, and D. Steingart, “Understanding Adverse Effects of Temperature Shifts on Li-Ion Batteries: An Operando Acoustic Study,” *J. Electrochem. Soc.*, vol. 167, no. 9, p. 090503, 2020.
 - [19] P. Daponte, G. Fazio, and A. Molinaro, “Detection of echoes using time-frequency analysis techniques,” *Instrum. Meas. IEEE Trans.*, vol. 45, no. 1, pp. 30–40, 1996.
 - [20] L. Angrisani, P. Daponte, and M. D’Apuzzo, “The detection of echoes from multilayer structures using the wavelet transform,” *IEEE Trans. Instrum. Meas.*, vol. 49, no. 4, pp. 727–731, 2000.
 - [21] A. Grinsted, J. C. Moore, and S. Jevrejeva, “Application of the cross wavelet transform and wavelet coherence to geophysical time series,” *Nonlinear Process. Geophys.*, vol. 11, no. 5/6, pp. 561–566, Nov. 2004.